Anthropogenic impacts on amplified midlatitude European summer warming and rapid increase of heatwaves in recent decades

Geophysical Research Letters

RESEARCH LETTER
10.1029/2024GL108982

Anthropogenic Impacts on Amplified Midlatitude European Summer Warming and Rapid Increase of Heatwaves in Recent Decades

Zejiang Yin[1], Buwen Dong[2], Wei Wei[1,3], and Song Yang[1,3]

[1]School of Atmospheric Sciences, Sun Yat-sen University and Southern Marine Science and Engineering Guangdong Laboratory (Zhuhai), Zhuhai, China, [2]National Centre for Atmospheric Science, Department of Meteorology, University of Reading, Reading, UK, [3]Guangdong Province Key Laboratory for Climate Change and Natural Disaster Studies, Sun Yat-sen University, Zhuhai, China

Key Points:

- Midlatitude Europe exhibits more rapid increases in summer heatwave frequency than the global land averages in recent decades
- Atmospheric circulation changes contributing about one third of the observed warming trend, further intensify the rapid increases in summer heatwave frequency
- Local air temperature response to reduced aerosol emissions contributes about half of the enhanced warming compared to the global land average

Supporting Information:

Supporting Information may be found in the online version of this article.

Correspondence to:

S. Yang,
yangsong3@mail.sysu.edu.cn

Citation:

Yin, Z., Dong, B., Wei, W., & Yang, S. (2024). Anthropogenic impacts on amplified midlatitude European summer warming and rapid increase of heatwaves in recent decades. *Geophysical Research Letters*, *51*, e2024GL108982. https://doi.org/10.1029/2024GL108982

Received 26 FEB 2024
Accepted 8 AUG 2024

Abstract Midlatitude Europe (ME) emerges as a prominent heatwave hotspot with rapid increases in summer surface air temperature and heatwave days since 1979, surpassing the global land averages by approximately 2.6 and 2.3 times, respectively. The circulation analogs-based dynamic adjustment reveals that approximately 38% and 35% of these trends result from shifts in zonal dipolar circulation patterns over the North Atlantic (NA) and Europe, crucial for the enhanced warming compared to the global land average. The circulation changes are associated with warming sea surface temperatures in the NA. This warming pattern resembles the Atlantic Multidecadal Variability and is predominantly induced by greenhouse gases. Moreover, the stronger air temperature response in ME to decreased aerosols amplifies warming, contributing to the rapid increase in heatwave frequency. These findings highlight a prominent influence of anthropogenic forcings on the swift surge of European heatwaves compared to global land, with a potential implication for adaptation strategies and risk management.

Plain Language Summary Midlatitude Europe is experiencing a significant increase in heatwaves, with summer temperatures and heatwave occurrences rising much faster than the global land averages since 1979. One of the key contributors to this rapid warming is the changes in zonal dipolar circulation patterns over the NA and Europe, which are linked to the warm sea surface temperatures in the NA. This warming pattern, resembling the Atlantic Multidecadal Variability, is largely caused by greenhouse gases and additionally influenced by reduced aerosols and natural forcing. Furthermore, the stronger response of air temperatures in midlatitude Europe to decreased aerosol emissions intensifies summer warming, contributing to a rapid increase in heatwave days. These findings highlight the significant impact of anthropogenic forcings on the observed surge of heatwaves in Europe compared to global land, with an important implication for developing strategies to adapt to these changing climate conditions and managing the associated risks.

1. Introduction

The summer surface air temperature over Eurasia exhibits a non-uniform pattern of changes, superimposed on a general warming trend, revealing remarkably amplified warming trends over Europe in recent decades (Dong et al., 2017; X. Hong et al., 2017; Hua et al., 2021; Singh et al., 2023; Teng et al., 2022; Vautard et al., 2023). Concurrent with this rapid warming, Europe has experienced a series of severe heatwaves during the 21st century (Russo et al., 2015), characterized by a recent cluster of consecutive heatwaves including those in 2003 (Stott et al., 2004), 2010 (Dole et al., 2011), 2015 (Mecking et al., 2019), 2018 (Li et al., 2020), 2019 (Sanchez-Benitez et al., 2022), and 2022 (Iacobucci, 2023). Additionally, European heatwaves are anticipated to increase disproportionately faster compared to the global mean temperature in the future (Russo et al., 2015). The frequent occurrence of severe and persistent heatwaves is of critical concern for the society due to their association with wildfires (Sutanto et al., 2020), air pollution (Garrido-Perez et al., 2019), extensive crop failure (Lesk et al., 2016), and increased mortality (CRED, 2020). Therefore, understanding why Europe is warming faster than other regions is important and essential for improving climate predictions and risk assessments.

Changes in European summer surface air temperatures and heatwaves are influenced by a combination of dynamic drivers, such as anticyclonic circulation and jet stream states (Deng et al., 2018; Horton et al., 2015; Rousi et al., 2022; Singh et al., 2023; Vautard et al., 2023) and thermodynamic drivers including radiative

forcing and land-atmosphere feedbacks (Seneviratne et al., 2010; Singh et al., 2023; Vautard et al., 2023). Anthropogenic forcings may lead to the warming trends by affecting both thermodynamic and dynamic drivers (Suarez-Gutierrez et al., 2020). Thus, the amplified warming in Europe may, in part, stem from the regional changes in the dynamic and thermodynamic effects in response to anthropogenic forcings. Since the 1980s, industrialized countries, including European countries, have undergone a substantial reduction in anthropogenic aerosol emissions due to stringent air pollution legislation (Smith & Bond, 2014). Aerosol particles, characterized by a short average residence time (between a day and a week), prompt localized forcing and a rapid response of atmospheric aerosol burden to emission changes (Navarro et al., 2016). This phenomenon can contribute to the amplified warming over Europe through aerosol–radiation and aerosol–cloud interactions (Dong et al., 2017, 2023; Tian et al., 2020). Additionally, given their uneven spatial distribution, aerosols can induce alterations in both horizontal and vertical temperature gradients, consequently influencing atmospheric circulation and air temperatures (Dong & Sutton, 2021; Undorf et al., 2018). This interconnected relationship between dynamic drivers and anthropogenic influences, underscores the complexity of the factors shaping European climate patterns and heatwaves.

In addition to the anthropogenically driven changes, internal variability in the climate system can alter the warming rate in Europe. Previous studies have emphasized the substantial role of the Atlantic Multidecadal Variation (AMV) in European warming (Dong & Sutton, 2021; Dong et al., 2017; Ghosh et al., 2019; X. Hong et al., 2017; Luo et al., 2023; Sutton & Dong, 2012; Sutton & Hodson, 2005). The AMV could influence regional climate through its induced atmospheric circulations (Ghosh et al., 2019; Luo et al., 2023; Sutton & Dong, 2012; Sutton & Hodson, 2005) and may drive decadal changes in the Silk Road Pattern, resulting in non-uniform Eurasian warming (X. Hong et al., 2017; Si & Ding, 2016; Sun et al., 2019; L. Wang et al., 2017). More complicated, the recent AMV is a consequence of both internal variability and anthropogenic forcing (Ottera et al., 2010; Qin et al., 2020a, 2020b; Steinman et al., 2015; Watanabe & Tatebe, 2019). Consequently, the drivers and underlying physical processes responsible for the notably faster European warming in recent decades, especially regarding heatwave frequency, have not been fully addressed.

Luo et al. (2023) revealed that increased European heatwaves in recent decades was due to the combined effect of GHG-induced warming and a cold-to-warm phase shift of AMO-like variations. Here, we further discuss the dynamic and thermodynamic processes that have made midlatitude Europe (ME) a hotspot, experiencing faster summer warming and rapid increasing heatwave days (HDs) compared to those over global land. We employ an observation-based dynamic adjustment method to assess the dynamics and thermodynamics contributions to the multidecadal changes of European daily maximum surface air temperature (TX) and estimate these contributions to the change in HDs. Additionally, a set of climate model simulations in the Coupled Model Intercomparison Project Phase 6 (CMIP6) is utilized to offer insights into the impacts of anthropogenic greenhouse gases forcing (GHG), anthropogenic aerosols forcing (AA), and natural forcing (NAT) on the TX and HDs, along with the drivers behind the recent AMV-like sea surface temperature (SST) warming. These findings may contribute to constraining the future changes in heatwaves and, consequently, designing effective adaptation and resilience plans.

2. Data and Methods

2.1. Observational Data and Model Simulations

The daily data, spanning from 1950 to 2022, were acquired from the ERA5 reanalysis (Hersbach et al., 2020), including horizontal winds and geopotential height at 500 hPa (Z500), and TX. Monthly SST data were obtained from the Hadley Center HadISST (Rayner et al., 2003). Monthly aerosol optical depth (AOD) at wavelength of 550 nm was provided by the MERRA2 reanalysis (Gelaro et al., 2017).

Ensemble simulations from nine models in CMIP6 were examined (Table S1 in Supporting Information S1; Eyring et al., 2016), each comprising at least three ensemble members for different forcing scenarios: anthropogenic and natural forcings (ALL), GHG only, AA only, and NAT only during 1850–2014 (or 1850–2020). Historical ALL simulations were extended to 2022 using Shared Socioeconomic Pathway 3–7.0 simulations (using Shared Socioeconomic Pathway 2–4.5 simulations for HadGEM3-GC31-LL). Prior the analysis, all model data were bi-linearly interpolated to a common resolution of 1.0° × 1.0°.

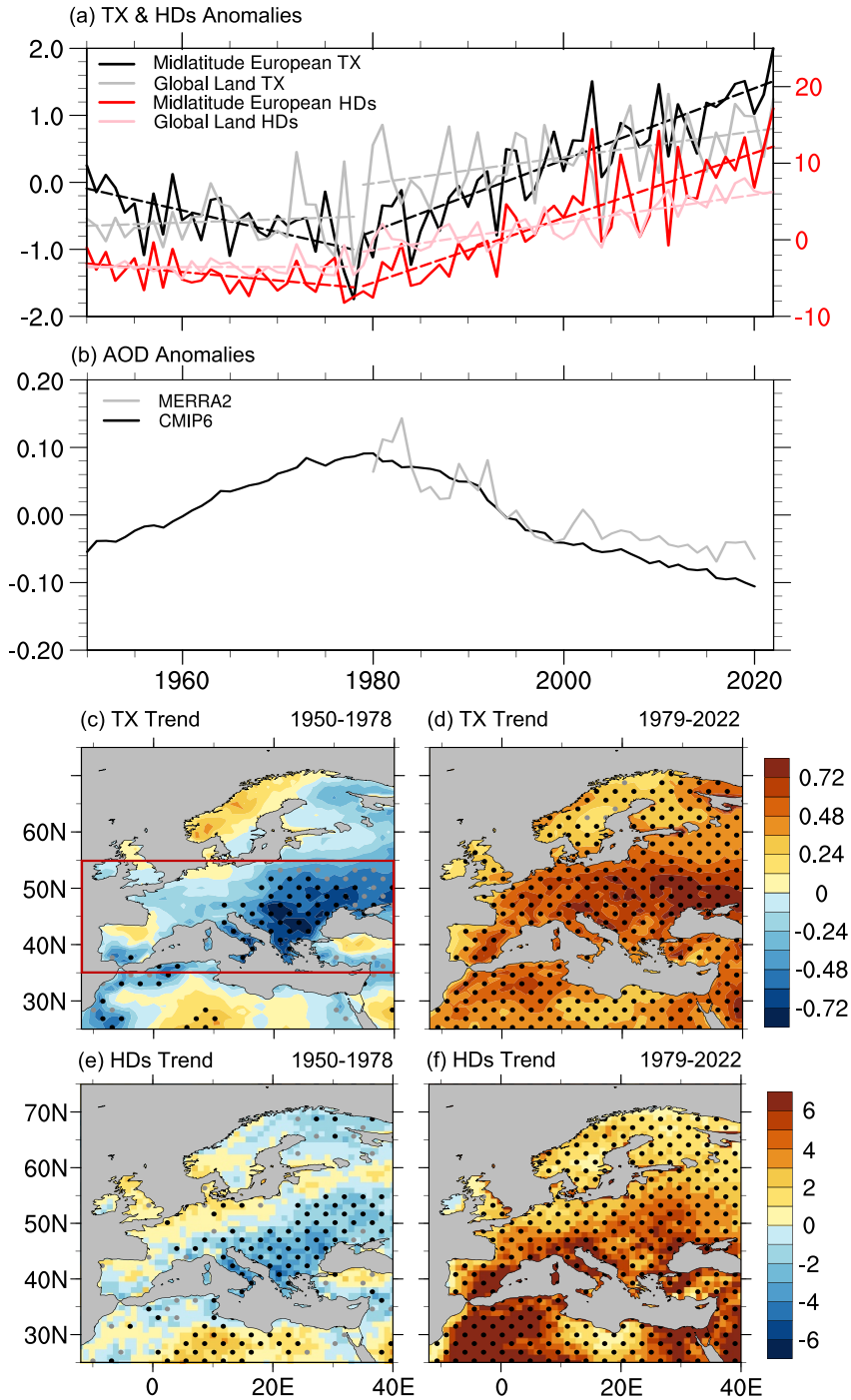

Figure 1. (a) Time series of summer (June-July-August) TX (°C) and heatwave days (HDs) (day) anomalies over midlatitude Europe (ME; black solid and red solid lines) and global land (gray solid and pink solid lines). Linear trends during 1950–1978 and 1979–2022 are represented by dashed lines. (b) Time series of summer aerosol optical depth from MERRA2 reanalysis and MMM of AA simulations. Spatial patterns of trends in (c)–(e) TX (°C decade^{-1}) and (d)–(f) HD (day decade^{-1}) during the two periods. Gray and black dots indicate the trends that are statistically significant at the 0.1 and 0.05 level, respectively.

2.2. Methods

The study is focused on ME within the domain of 35°–55°N, 12°W–40°E (Figure 1b). Heatwaves are defined when daily TX exceeds the relative threshold for at least 3 days. The relative threshold on each calendar day is

computed as the daily 90th percentile of TX based on 15-day samples centered on that day during the baseline period of 1950–1979. Summer HDs are the sum of all HDs in June-July-August. Linear trends are calculated using a least squares regression analysis, and the significance is assessed with a two-tailed Student's *t*-test. Following Enfield et al. (2001), the AMV index is defined as the local linearly detrended 9-year low-pass-filtered summer mean SST anomalies averaged over the North Atlantic (NA, 80–0°W, 0°–60°N). A Lanczos filter with 13 points and 9-year cutoff period is used for low-pass filtering. Additionally, externally forced signals in the CMIP6 models are evaluated by averaging the single-model ensemble mean and then the multimodal ensemble mean (MMM).

A circulation analogs-based dynamical adjustment technique is employed to isolate the impacts of dynamics and thermodynamics on the multidecadal changes in European summer TX and HDs (Gong et al., 2024). This technique is described in detail in Deser et al. (2016) and briefly summarized below. We consider daily Z500 as a proxy variable of atmospheric circulations. The spatially averaged Z500 (10°–80°N, 60°W–60°E) is subtracted from the Z500 field at each time step and grid to mitigate the effect of thermal expansion. For each day, the top 100 circulation analogs (10°–80°N, 60°W–60°E) are chosen based on Euclidean distance within the 62-day window around the corresponding calendar day, excluding the year of occurrence of this day. From these 100 patterns, 50 are randomly sampled and combined in a linearly optimal way to construct a Z500 analog that resembles most closely to the Z500 pattern for the day of consideration. The derived coefficients are then applied to TX, forming the dynamically induced component. This process is repeated 100 times to prevent overfitting, and the average is dynamically-induced component. The thermodynamically-induced component is obtained by subtracting this component from the original TX. Before constructing analogs, Z500 and TX are detrended for each grid cell by eliminating the first intrinsic mode function of the ensemble empirical mode decomposition (Wu & Huang, 2009). The dynamical adjustment is also used in each member of the CMIP6 models, and the circulation analogs are chosen in piControl.

The dynamic contribution to the TX trends, induced by atmospheric circulation changes, is calculated as the ratio of the dynamically-induced trend to the total trends. The thermodynamically-induced trends are the difference between the total trends and the trends induced by atmospheric circulation changes. The thermodynamic contribution is the ratio of the thermodynamically-induced trends to the total trends. Both the dynamic and thermodynamic contributions can be influenced by external forcing and internal variability.

To estimate the contribution of changes in dynamically-induced summer TX to HDs, we subtract the cooling (warming) trends of dynamical components before 1978 (after 1979) from the original TX, and then calculate the HDs using the same relative threshold as in the original TX. The differences of trends between the original HDs and new calculated ones are attributed to the changes in dynamically-induced TX. The ratio of this trend to the total HDs trend is the dynamic contribution to the HDs trends. Similarly, we can estimate the thermodynamic contribution to the HDs trends.

3. Result

3.1. Amplified Warming Trends Over ME in Recent Decades

The summer TX anomalies averaged over ME exhibits remarkable V-shaped multidecadal changes, featuring a significant cooling trend of −0.31°C decade^{-1} during 1950–1978 and a subsequent rapid warming trend of 0.53°C decade^{-1} from 1979 to 2022 (Figure 1a). These trends correspond to an increase in AOD during the former period and a decreasing AOD trend during the latter period (Figure 1b). During the cooling period, the cooling trends of TX are widespread across ME, with the most pronounced values in southern and central-eastern Europe (Figure 1c). In contrast, from 1979 to 2022, the warming trends displayed a spatial pattern mirroring the cooling period, with central-eastern Europe experiencing the most pronounced warming (Figure 1d). Concurrent with the changes in TX, the HDs over ME follow the similar V-shaped multidecadal changes, with a decrease trend before 1978 (−1.1 day decade^{-1}) and a rapid increase trend after 1979 (4.3 day decade^{-1}). The spatial distribution of HD trends also aligns with that of TX during both periods (Figures 1e and 1f). Particularly, during recent decades (1979–2022), the rapid increasing trends of TX and HDs over ME are respectively 2.7 and 2.4 times of the global land averages. The enhanced trends are particularly pronounced across central-eastern Europe (Figure S1 in Supporting Information S1). Consequently, ME emerges as a hotspot, experiencing a notably intensified trend in summer TX and HDs during the recent decades of 1979–2022.

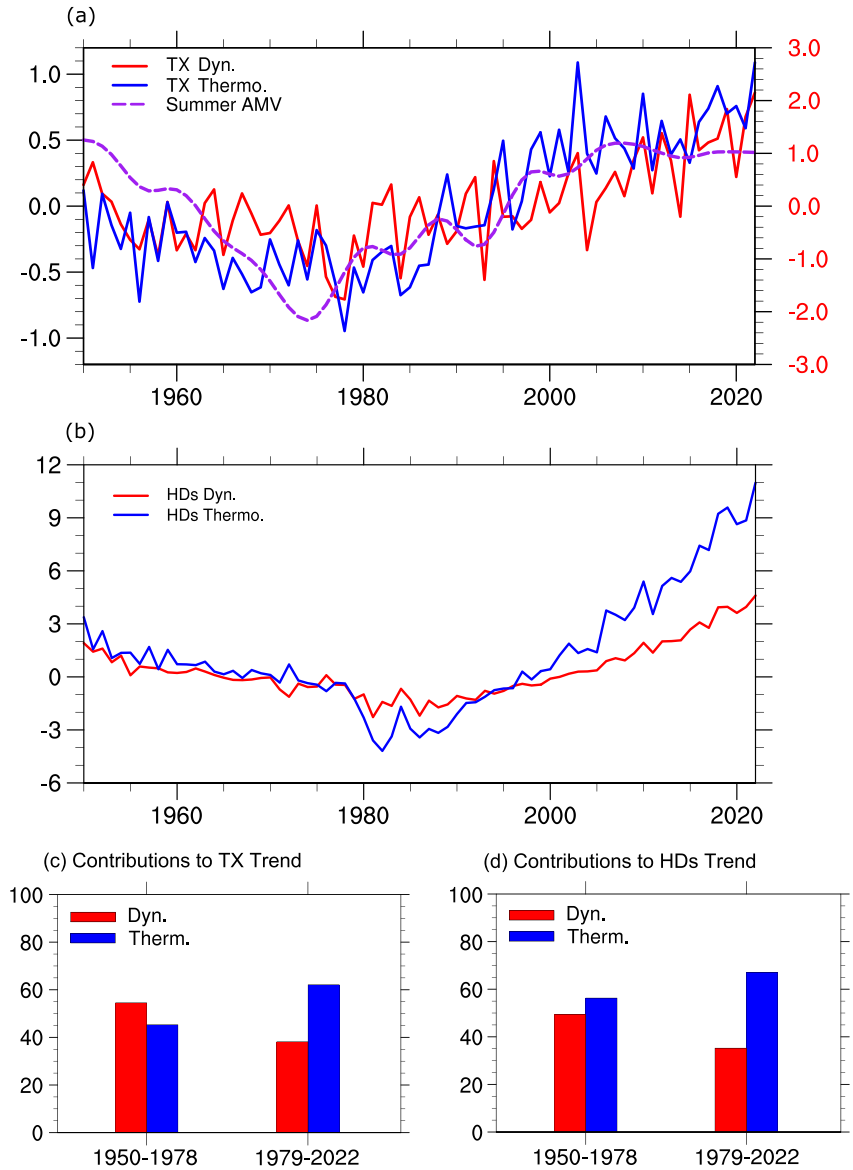

Figure 2. (a) Time series of dynamically-induced (red solid line) and thermodynamically-induced (blue solid line) TX over midlatitude Europe (ME), along with the standardized summer Atlantic Multidecadal Variation index (purple dash line). (b) Time series of the heatwave days (HDs) calculated from TX timeseries containing only thermodynamically-induced (blue line) or dynamically-induced (red line) trends. (c) Contributions (%) to the TX trends over ME during the two periods from the dynamic component (red bar) and thermodynamic component (blue bar). Panel (d) is the same as (c), but for HDs. Both (b) and (d) averaged over the sub-region with significant TX trends at the 0.1 level over ME in Figures 1c and 1d.

3.2. Contribution of Dynamical and Thermodynamical Processes to Amplified Warming

To illustrate the contributions of dynamic and thermodynamic processes to the amplified warming trends in ME, we employ a dynamic adjustment approach based on observed daily Z500. Both dynamically- and thermodynamically-induced TX trends show V-shaped multidecadal changes during 1950–2022 (Figure 2a). Specifically, during the cooling period, the dynamically-induced trend (−0.17°C decade^{-1}) contributes about 55% of the observed TX trend (red bar in Figure 2c), with a spatial pattern showing large contributions in southern and central-eastern Europe (Figure S2a in Supporting Information S1). During 1979–2022, 38% of the observed warming trend results from the dynamic processes (0.2°C decade^{-1}; Figure 2c), consistent with Singh et al. (2023). These trends intensify from western Europe to central-eastern Europe (Figure S2c in Supporting Information S1). In both periods, the spatial pattern of the dynamically-induced trends closely aligns with the total

trends over ME, with spatial correlation coefficients of 0.77 and 0.81, larger than those between the thermodynamically components and the total trends (0.52 and 0.57; Figures S2b and S2d in Supporting Information S1).

The dynamically-induced TX trends contribute approximately 49% (35%) of the total HD trends before 1978 (after 1979) over the sub-regions with significant TX trends in ME during each period (Figures 2b and 2d). The spatial patterns of these trends closely mirror the total trends during both periods over ME (Figures S3a and S3c in Supporting Information S1), with spatial correlation coefficients of 0.71 and 0.85, larger than that of thermodynamically components (0.56 and 0.72; Figures S3b and S3d in Supporting Information S1). These results indicate the crucial role of dynamic processes in the nonuniform distribution of TX and HD multidecadal changes.

However, even under the assumption that the dynamically-induced TX (HD) trends averaged over global land is close to zero, the dynamical processes could only contribute about 52% (48%) to the enhanced component of TX (HD) trends over ME. This enhanced component is defined as the trends over ME minus those of the global land average. Additionally, the thermodynamically-induced TX (HD) trend over ME is 0.33°C decade^{-1} (2.9 day decade^{-1}), also exceeds the global averages of 0.20°C decade^{-1} (1.5 day decade^{-1}). Thus, the faster warming trends over ME may be controlled by both dynamical and thermodynamical processes.

3.3. Impact of AMV-Like SST Warming on Dynamically-Induced Warming

To better comprehend the impact of circulation changes on the rapid warming trend, we further elucidate the possible mechanisms. Figures 3a and 3b reveal a dipole trend pattern of Z500, mirroring each other during both periods. During 1979–2022, circulation trends show a cyclonic pattern over the NA, coinciding with an anticyclonic pattern over Europe (Figure 3b). This anticyclonic anomaly is crucial for summer TX and the occurrence of heatwaves via facilitating the advection of warm air on the western side of the system, subsidence, and increased solar radiation due to reduced cloudiness (Trigo et al., 2005). The zonal dipole patterns are coherent with the atmospheric anomalies related to AMV on the decadal timescale, as illustrated by Luo et al. (2023, their Figure 8c). Additionally, the AMV index also exhibits a V-shaped multidecadal variability (purple dash line in Figure 2a), indicating a close relationship between AMV and the dipolar pattern of circulation changes. Both dynamic diagnosis and model numerical simulation suggest that the positive AMV can induce an anomalous anticyclonic circulation over Europe (H. Hong et al., 2020; Hua et al., 2021; Si & Ding, 2016). Furthermore, the dynamically-induced TX and HDs regressed onto the AMV index show significant and positive anomalies over most ME (Figures S4a and S4c in Supporting Information S1), and the spatial patterns exhibit similar features to the dynamically-induced trends over ME during the both periods (Figures S2 and S3 in Supporting Information S1), suggesting that the AMV could influences the TX and HDs through dynamical processes.

Additionally, the NA SST trends during 1979–2022 exhibit an AMV-like warming pattern, characterized by pronounced warming in the mid-higher latitude NA (Figure S5b in Supporting Information S1). To investigate the associated circulation anomalies, we employ the atmospheric component of the Community Earth System Model version 1.2.2 (Hurrell et al., 2013). Our analysis includes a 40-year control simulation forced by the global climatology of monthly-mean SSTs and sea-ice concentrations from the Hadley Center (Rayner et al., 2003), and a sensitivity experiment, in which the anomalies equivalent to two-fold of the monthly AMV-like SST (80–0°W, 20°–60°N) warming trends are added onto the monthly climatological SSTs during summer. The differences in circulation pattern between the sensitivity and control experiments exhibit a dipolar pattern, albeit weaker than the observed, and cyclonic anomalies slightly eastward (Figure S6a in Supporting Information S1).

We further demonstrate the influence of internal variability and external forcing on the AMV-like SST changes. A linear regression analysis is conducted between observed SST and the NA SST time series (80–0°W, 0°–60°N) from the MMM of ALL simulations (9 models; Table S1 in Supporting Information S1) during 1950–2022 to estimate the externally-forced component in observed SSTs over the NA (Steinman et al., 2015). The internally-generated component is obtained by subtracting the externally-forced component from the observed SST at each grid point. During 1950–1978, the AMV-like SST cooling is predominantly attributed to internal variability (Figure S5e in Supporting Information S1), with a modest response to external forcing that could be attributed to AA-forced cooling offsetting GHG-induced warming (Figure 3d and Figure S5c in Supporting Information S1). However, during 1979–2022, the observed AMV-like SST warming trend is comparable to the externally-forced SST trend dominated by increased GHG and further amplified by decreased aerosol emissions and natural forcing (Figures 3c and 3d; Figures S5b, S5d, and S5f in Supporting Information S1). In summary, the AMV-like

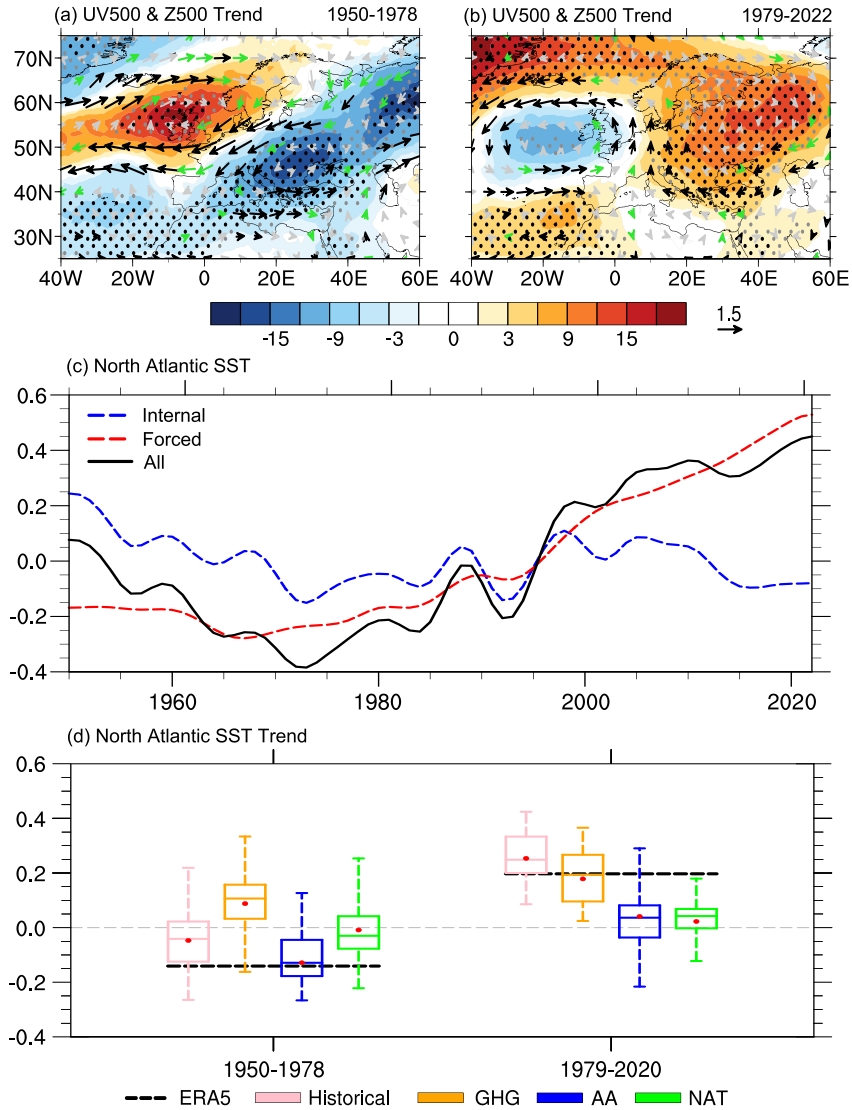

Figure 3. Spatial patterns of trends in horizontal wind (m s^{-1} $decade^{-1}$, vectors) and geopotential height (gpm $decade^{-1}$, shading) at 500 hPa in summer during (a) 1950–1978 and (b) 1979–2022. Gray (green) and black (black) dots (vectors) mark the significant values exceeding the 0.1 and 0.05 significance levels, respectively. (c) Time series of 9-year low-pass filtered, summer North Atlantic (NA) sea surface temperature (SST) anomalies (°C) for observations (black), externally forced component (red) and internal variability component (blue). (d) The summer NA SST trends (°C $decade^{-1}$) from MMM of ALL (pink), GHG (yellow), AA (blue) and NAT (green) simulations. Black dash lines represent the observed SST trends. Red dots indicate the MMM values. The box is the 25th and 75th percentile range, with the inside line for the median, and the whiskers for the maximum and minimum values.

warming since 1979, dominated by external forcing, could lead to the zonal dipolar circulation changes and accelerate the warming trend over ME.

3.4. Contribution of Decreased Aerosol Emissions to Amplified Warming

Hereafter, we analyze TX and HDs trends in the CMIP6 models to gain insights into the impacts of external forcing. The externally forced trends from 1979 to 2020 in CMIP6 mirror those during 1979–2022 and are comparable to the observed trends (gray and red bars in Figures 4a and 4c), suggesting that the amplified trends over ME during 1979–2022 are dominated by external forcing. However, the MMM of ALL displays weaker dynamically-induced and stronger thermodynamically-induced trends than the observed ones (gray and red bars in Figures 4e and 4f). These discrepancies may arise from the systematic biases in simulations or internal

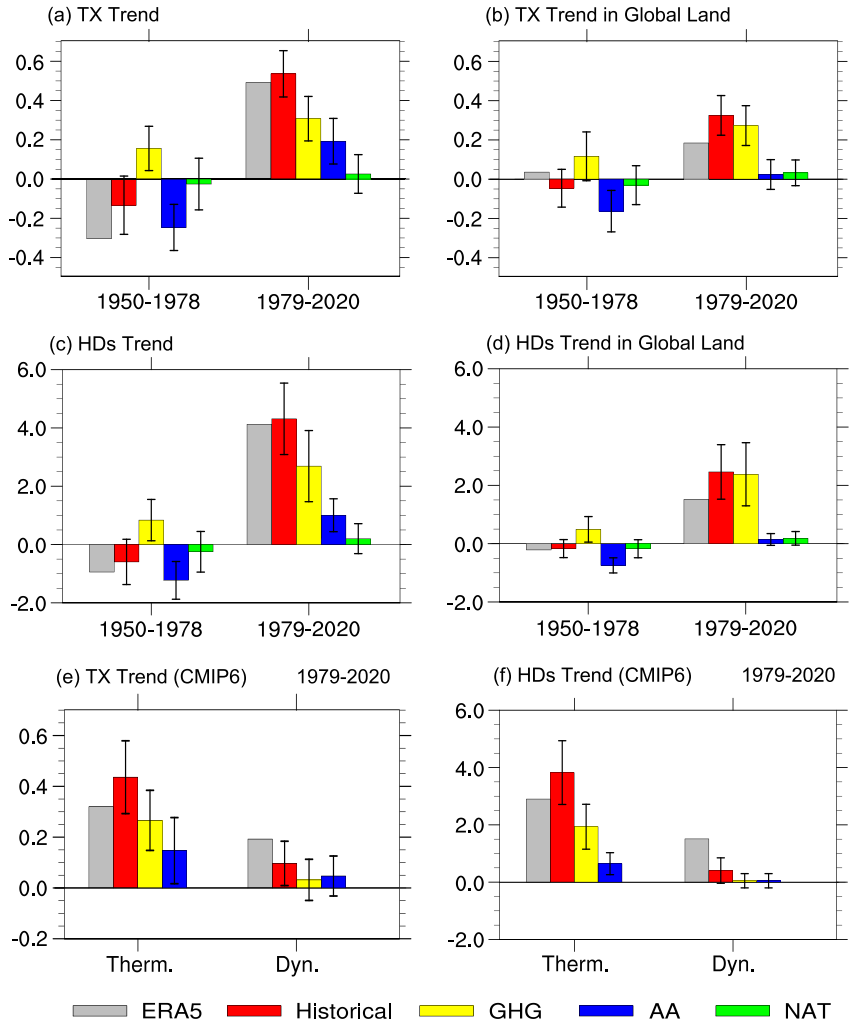

Figure 4. (a) TX and (c) heatwave day (HD) trends over midlatitude Europe from ERA5 (gray), and the MMM of ALL (red), GHG (yellow), AA (blue) and NAT (green) simulations. Error bars denote the standard deviation of inter-model variations. Panels (b) and (d) are the same as (a) and (c), respectively, but for the global land averages. Dynamic and thermodynamic component of (e) TX and (f) HD trends since 1979 are from ERA5 and the MMM of ALL, GHG and AA simulations.

variability in observations. Almost all of the ALL simulations exhibit weaker dynamical and stronger thermodynamic contributions. This systematically weaker dynamically-induced trends may be related to the weaker dipolar circulation response to external forcing (Figure S6b in Supporting Information S1). Moreover, the MMM of TX (HD) trends over ME in ALL are about 1.7 (1.8) times the global land averages, substantially weaker than the observed 2.6 (2.3). This discrepancy likely arises from the systematically underestimated circulation response and overestimated thermodynamic response to external forcing in the CMIP6 models.

To further explore the influences of different forcings on shaping enhanced component of warming over ME, we conduct a further analysis of the additional model simulations forced by GHG, AA, and NAT individually. The MMM of GHG simulations highlights the predominant role of increased GHG concentrations in driving the warming trends in TX and HDs over ME during 1979–2020 (Figures 4a and 4c), consistent with Luo et al. (2023). However, these trends are comparable to those observed over global land (Figure 4 and Figure S7 in Supporting Information S1). As discussed in Section 1, substantially reduced anthropogenic emissions of aerosols and their precursor gases over Europe in the recent decades (Lund et al., 2023, their Figure S1; Y. Wang et al., 2015, their Figure 1), associated with decreased AOD as revealed in both observations and simulations (Figure 1b; Hammer et al., 2018; Lund et al., 2023), have amplified the warming trend in this region. Although AA generally causes surface cooling relative to the pre-industrial period, the decrease in AA since 1980s has resulted in less cooling in

recent years compared to the earlier periods, leading to warming trends. In responses to the decreased aerosol emissions, the TX (HDs) increased faster over ME than over global land during 1979–2020 (Figure 4 and Figure S7 in Supporting Information S1), contributing approximately 51% (45%) to the enhanced component of TX (HD) trends over ME. This important role of AA changes is further supported by the accelerated cooling trends during 1950–1978 compared to those over global land, accompanied by increased aerosol emissions (Figure 4). Furthermore, the dynamic adjustment from the AA simulations indicates that the warming response over ME since 1979 is dominated by thermodynamic processes (Figures 4e and 4f). Consistent with previous research (Dong et al., 2017; Nabat et al., 2014; Ruckstuhl et al., 2010; Tian et al., 2020), the reduction of aerosol emissions could affect European surface air temperature primarily through aerosol-radiation interaction, with additional contributions from aerosol-cloud interaction (Figure S8 in Supporting Information S1). Thus, the decreased aerosol emissions since 1980s may be an important additional driver for the enhanced component of TX and HD trends over ME.

4. Summary and Discussion

Summer TX and HDs over ME display distinctive changes compared to the global land since 1950, characterized by decreased trends before 1978 and emerging as a heatwave hotspot after 1979. These warming trends are about 2.6 and 2.3 times higher than the global land averages, respectively. Utilizing a dynamical adjustment method based on observations, approximately 38% (35%) of the TX (HD) trend during 1979–2022 can be attributed to the circulation changes that are characterized by a zonal dipolar pattern, with a cyclonic over NA and an anticyclonic over Europe. This pattern is closely related to the externally forced AMV-like SST warming. The SST warming is largely attributed to increased GHG and further amplified by the reduced aerosol emissions and natural forcing. Furthermore, the MMM in ALL simulations could captures the dipolar circulation changes as observed, albeit notably weaker. This feature may be one of the reasons for the systematically underestimated trends in dynamically-induced TX and HDs in the simulations.

CMIP6 simulations show that about half of the enhanced component of TX (HD) trends over ME relative to the global land average can be attributed to the more pronounced air temperature response to the decreased aerosols, primarily arising from thermodynamic processes. Moreover, the zonal dipolar circulation changes, also related to external forcing, further amplified this enhanced component. Given the important impact of external forcing on summer warming and heatwaves over ME in the recent decades, improving the accuracy of decadal predictions for heatwaves in the upcoming years are conceivable by considering estimated near-future changes in GHG and AA. Our findings should help uncover the nature and cause of the recent amplified summer warming over ME and to project whether Europe will experience more warming in the future. However, the potential underestimation of circulation response and overestimation of thermodynamic response to external forcing in models hinder a full understanding of the roles of external forcing and internal variability in the observed amplified ME warming and associated rapid increase in heatwaves. The response of circulation to external forcing may be different in future, and the state-of-the-art models still face uncertainties in simulating the circulation response to a given AA and GHGs forcing. These questions need to be further investigated.

Conflict of Interest

The authors declare no conflicts of interest relevant to this study.

Data Availability Statement

The ERA5 reanalysis is provided by the European Centre for Medium-range Weather Forecast via Hersbach, H. et al. (2023). The HadISST data set is obtained from the Hadley Center HadISST via Rayner et al. (2003). The CMIP6 data sets are archived from https://esgf-node.llnl.gov/search/cmip6/.

Acknowledgments
The authors are grateful to all data providers. This research was supported by the Innovation Group Project of Southern Marine Science and Engineering Guangdong Laboratory (Zhuhai) (Grant 311021001), the Guangdong Major Project of Basic and Applied Basic Research (Grant 2020B0301030004), the Guangdong Province Key Laboratory for Climate Change and Natural Disaster Studies (Grant 2020B1212060025), and International Program for Ph.D. Candidates (Sun Yat-sen University). BD is supported by the UK National Centre for Atmospheric Science, funded by the Natural Environment Research Council (NERC) and BD's contribution to this work is supported by the NERC grant "Climate change in the Arctic-North Atlantic Region and Impacts on the UK (CANARI)" (NE/W004984/1). The authors would like two anonymous reviewers for their valuable comments and suggestions on the early version of the manuscript.

References

CRED. (2020). *Natural disasters 2019: Now is the time to not give up* (p. 8). Centre for Research on the Epidemiology of Disasters. Retrieved from https://cred.be/sites/default/files/adsr_2019.pdf

Deng, K., Yang, S., Ting, M., Lin, A., & Wang, Z. (2018). An intensified mode of variability modulating the summer heat waves in eastern Europe and northern China. *Geophysical Research Letters*, *45*(20), 11361–11369. https://doi.org/10.1029/2018GL079836

Deser, C., Terray, L., & Phillips, A. S. (2016). Forced and internal components of winter air temperature trends over North America during the past 50 years: Mechanisms and implications. *Journal of Climate*, *29*(6), 2237–2258. https://doi.org/10.1175/jcli-d-15-0304.1

Dole, R., Hoerling, M., Perlwitz, J., Eischeid, J., Pegion, P., Zhang, T., et al. (2011). Was there a basis for anticipating the 2010 Russian heat wave? *Geophysical Research Letters*, *38*(6), L06702. https://doi.org/10.1029/2010gl046582

Dong, B., & Sutton, R. T. (2021). Recent trends in summer atmospheric circulation in the North Atlantic/European region: Is there a role for anthropogenic aerosols? *Journal of Climate*, *34*(16), 6777–6795. https://doi.org/10.1175/jcli-d-20-0665.1

Dong, B., Sutton, R. T., & Shaffrey, L. (2017). Understanding the rapid summer warming and changes in temperature extremes since the mid-1990s over Western Europe. *Climate Dynamics*, *48*(5–6), 1537–1554. https://doi.org/10.1007/s00382-016-3158-8

Dong, B., Sutton, R. T., & Wilcox, L. J. (2023). Decadal trends in surface solar radiation and cloud cover over the North Atlantic sector during the last four decades: Drivers and physical processes. *Climate Dynamics*, *60*(7–8), 2533–2546. https://doi.org/10.1007/s00382-022-06438-3

Enfield, D. B., Mestas-Nuñez, A. M., & Trimble, P. J. (2001). The Atlantic Multidecadal Oscillation and its relation to rainfall and river flows in the continental US. *Geophysical Research Letters*, *28*(10), 2077–2080. https://doi.org/10.1029/2000gl012745

Eyring, V., Bony, S., Meehl, G. A., Senior, C. A., Stevens, B., Stouffer, R. J., & Taylor, K. E. (2016). Overview of the coupled model intercomparison project phase 6 (CMIP6) experimental design and organization. *Geoscientific Model Development*, *9*(5), 1937–1958. https://doi.org/10.5194/gmd-9-1937-2016

Garrido-Perez, J. M., Ordonez, C., Garcia-Herrera, R., & Schnell, J. L. (2019). The differing impact of air stagnation on summer ozone across Europe. *Atmospheric Environment*, *219*, 117062. https://doi.org/10.1016/j.atmosenv.2019.117062

Gelaro, R., McCarty, W., Suárez, M. J., Todling, R., Molod, A., Takacs, L., et al. (2017). The modern-era retrospective analysis for research and applications, version 2 (MERRA-2). *Journal of Climate*, *30*(14), 5419–5454. https://doi.org/10.1175/jcli-d-16-0758.1

Ghosh, R., Mueller, W. A., Eichhorn, A., Baehr, J., & Bader, J. (2019). Atmospheric pathway between atlantic multidecadal variability and European summer temperature in the atmospheric general circulation model ECHAM6. *Climate Dynamics*, *53*(1–2), 209–224. https://doi.org/10.1007/s00382-018-4578-4

Gong, H., Ma, K., Hu, Z., Dong, Z., Ma, Y., Chen, W., et al. (2024). Attribution of the August 2022 extreme heatwave in southern China: Role of dynamical and thermodynamical processes. *Bulletin of the American Meteorological Society*, *105*(1), E193–E199. https://doi.org/10.1175/BAMS-D-23-0175.1

Hammer, M. S., Martin, R. V., Li, C., Torres, O., Manning, M., & Boys, B. L. (2018). Insight into global trends in aerosol composition from 2005 to 2015 inferred from the omi ultraviolet aerosol index. *Atmospheric Chemistry and Physics*, *18*(11), 8097–8112. https://doi.org/10.5194/acp-18-8097-2018

Hersbach, H., Bell, B., Berrisford, P., Hirahara, S., Horányi, A., Muñoz-Sabater, J., et al. (2020). The ERA5 global reanalysis. *Quarterly Journal of the Royal Meteorological Society*, *146*(730), 1999–2049. https://doi.org/10.1002/qj.3803

Hersbach, H., Bell, B., Berrisford, P., Hirahara, S., Horányi, A., Muñoz-Sabater, J., et al. (2023). *ERA5 monthly averaged data on pressure levels from 1940 to present*. Copernicus Climate Change Service (C3S) Climate Data Store (CDS). https://doi.org/10.24381/cds.6860a573

Hong, H., Sun, J., & Wang, H. (2020). Interdecadal variation in the frequency of extreme hot events in Northeast China and the possible mechanism. *Atmospheric Research*, *244*, 105065. https://doi.org/10.1016/j.atmosres.2020.105065

Hong, X., Lu, R., & Li, S. (2017). Amplified summer warming in Europe-West Asia and Northeast Asia after the mid-1990s. *Environmental Research Letters*, *12*(9), 094007. https://doi.org/10.1088/1748-9326/aa7909

Horton, D. E., Johnson, N. C., Singh, D., Swain, D. L., Rajaratnam, B., & Diffenbaugh, N. S. (2015). Contribution of changes in atmospheric circulation patterns to extreme temperature trends. *Nature*, *522*(7557), 465–469. https://doi.org/10.1038/nature14550

Hua, W., Qin, M., Dai, A., Zhou, L., Chen, H., & Zhang, W. (2021). Reconciling human and natural drivers of the tripole pattern of multidecadal summer temperature variations over Eurasia. *Geophysical Research Letters*, *48*(14), e2021GL093971. https://doi.org/10.1029/2021gl093971

Hurrell, J., Holland, M., Gent, P., Kay, J., Kushner, P., Lamarque, J., et al. (2013). The community earth system model: A framework for collaborative research. *Bulletin of the American Meteorological Society*, *94*(9), 1339–1360. https://doi.org/10.1175/BAMS-D-12-00121.1

Iacobucci, G. (2023). Europe's record heatwave in 2022 caused many health harms, report finds. *BMJ*, *381*, p905. https://doi.org/10.1136/bmj.p905

Lesk, C., Rowhani, P., & Ramankutty, N. (2016). Influence of extreme weather disasters on global crop production. *Nature*, *529*(7584), 84–87. https://doi.org/10.1038/nature16467

Li, M., Yao, Y., Simmonds, I., Luo, D., Zhong, L., & Chen, X. (2020). Collaborative impact of the NAO and atmospheric blocking on European heatwaves, with a focus on the hot summer of 2018. *Environmental Research Letters*, *15*(11), 114003. https://doi.org/10.1088/1748-9326/aba6ad

Lund, M. T., Myhre, G., Skeie, R. B., Samset, B. H., & Klimont, Z. (2023). Implications of differences between recent anthropogenic aerosol emission inventories for diagnosed aod and radiative forcing from 1990 to 2019. *Atmospheric Chemistry and Physics*, *23*(12), 6647–6662. https://doi.org/10.5194/acp-23-6647-2023

Luo, B., Luo, D., Zhuo, W., Xiao, C., Dai, A., Simmonds, I., et al. (2023). Increased summer European heatwaves in recent decades: Contributions from greenhouse gases-induced warming and Atlantic Multidecadal Oscillation-like variations. *Earth's Future*, *11*(8), e2023EF003701. https://doi.org/10.1029/2023EF003701

Mecking, J. V., Drijfhout, S. S., Hirschi, J. J. M., & Blaker, A. T. (2019). Ocean and atmosphere influence on the 2015 European heatwave. *Environmental Research Letters*, *14*(11), 114035. https://doi.org/10.1088/1748-9326/ab4d33

Nabat, P., Somot, S., Mallet, M., Sanchez-Lorenzo, A., & Wild, M. (2014). Contribution of anthropogenic sulfate aerosols to the changing Euro-Mediterranean climate since 1980. *Geophysical Research Letters*, *41*(15), 5605–5611. https://doi.org/10.1002/2014gl060798

Navarro, J. C. A., Varma, V., Riipinen, I., Seland, O., Kirkevag, A., Struthers, H., et al. (2016). Amplification of Arctic warming by past air pollution reductions in Europe. *Nature Geoscience*, *9*(4), 277–281. https://doi.org/10.1038/ngeo2673

Ottera, O. H., Bentsen, M., Drange, H., & Suo, L. (2010). External forcing as a metronome for Atlantic Multidecadal Variability. *Nature Geoscience*, *3*(10), 688–694. https://doi.org/10.1038/ngeo955

Qin, M., Dai, A., & Hua, W. (2020a). Aerosol-forced multidecadal variations across all ocean basins in models and observations since 1920. *Science Advances*, *6*(29), eabb0425. https://doi.org/10.1126/sciadv.abb0425

Qin, M., Dai, A., & Hua, W. (2020b). Quantifying contributions of internal variability and external forcing to Atlantic Multidecadal Variability since 1870. *Geophysical Research Letters*, *47*(22), e2020GL089504. https://doi.org/10.1029/2020gl089504

Rayner, N. A., Parker, D. E., Horton, E. B., Folland, C. K., Alexander, L. V., Rowell, D. P., et al. (2003). Global analyses of sea surface temperature, sea ice, and night marine air temperature since the late nineteenth century. *Journal of Geophysical Research*, *108*(D14), 4407. https://doi.org/10.1029/2002jd002670

Rousi, E., Kornhuber, K., Beobide-Arsuaga, G., Luo, F., & Coumou, D. (2022). Accelerated Western European heatwave trends linked to more-persistent double jets over Eurasia. *Nature Communications*, *13*(1), 3851. https://doi.org/10.1038/s41467-022-31432-y

Ruckstuhl, C., Norris, J. R., & Philipona, R. (2010). Is there evidence for an aerosol indirect effect during the recent aerosol optical depth decline in Europe? *Journal of Geophysical Research*, *115*(D4), D04204. https://doi.org/10.1029/2009jd012867

Russo, S., Sillmann, J., & Fischer, E. M. (2015). Top ten European heatwaves since 1950 and their occurrence in the coming decades. *Environmental Research Letters*, *10*(12), 124003. https://doi.org/10.1088/1748-9326/10/12/124003

Sanchez-Benitez, A., Goessling, H., Pithan, F., Semmler, T., & Jung, T. (2022). The July 2019 European heat wave in a warmer climate: Storyline scenarios with a coupled model using spectral nudging. *Journal of Climate*, *35*(8), 2373–2390. https://doi.org/10.1175/jcli-d-21-0573.1

Seneviratne, S. I., Corti, T., Davin, E. L., Hirschi, M., Jaeger, E. B., Lehner, I., et al. (2010). Investigating soil moisture-climate interactions in a changing climate: A review. *Earth-Science Reviews*, *99*(3–4), 125–161. https://doi.org/10.1016/j.earscirev.2010.02.004

Si, D., & Ding, Y. (2016). Oceanic forcings of the interdecadal variability in East Asian summer rainfall. *Journal of Climate*, *29*(21), 7633–7649. https://doi.org/10.1175/jcli-d-15-0792.1

Singh, J., Sippel, S., & Fischer, E. M. (2023). Circulation dampened heat extremes intensification over the Midwest USA and amplified over Western Europe. *Communications Earth & Environment*, *4*(1), 432. https://doi.org/10.1038/s43247-023-01096-7

Smith, S. J., & Bond, T. C. (2014). Two hundred fifty years of aerosols and climate: The end of the age of aerosols. *Atmospheric Chemistry and Physics*, *14*(2), 537–549. https://doi.org/10.5194/acp-14-537-2014

Steinman, B. A., Mann, M. E., & Miller, S. K. (2015). Atlantic and Pacific multidecadal oscillations and Northern Hemisphere temperatures. *Science*, *347*(6225), 988–991. https://doi.org/10.1126/science.1257856

Stott, P. A., Stone, D. A., & Allen, M. R. (2004). Human contribution to the European heatwave of 2003. *Nature*, *432*(7017), 610–614. https://doi.org/10.1038/nature03089

Suarez-Gutierrez, L., Mueller, W. A., Li, C., & Marotzke, J. (2020). Dynamical and thermodynamical drivers of variability in European summer heat extremes. *Climate Dynamics*, *54*(9–10), 4351–4366. https://doi.org/10.1007/s00382-020-05233-2

Sun, X., Li, S., Hong, X., & Lu, R. (2019). Simulated influence of the Atlantic Multidecadal Oscillation on summer Eurasian nonuniform warming since the mid-1990s. *Advances in Atmospheric Sciences*, *36*(8), 811–822. https://doi.org/10.1007/s00376-019-8169-z

Sutanto, S. J., Vitolo, C., Di Napoli, C., D'Andrea, M., & Van Lanen, H. A. J. (2020). Heatwaves, droughts, and fires: Exploring compound and cascading dry hazards at the pan-European scale. *Environment International*, *134*, 105276. https://doi.org/10.1016/j.envint.2019.105276

Sutton, R. T., & Dong, B. (2012). Atlantic ocean influence on a shift in European climate in the 1990s. *Nature Geoscience*, *5*(11), 788–792. https://doi.org/10.1038/ngeo1595

Sutton, R. T., & Hodson, D. L. R. (2005). Atlantic ocean forcing of North American and European summer climate. *Science*, *309*(5731), 115–118. https://doi.org/10.1126/science.1109496

Teng, H., Leung, R., Branstator, G., Lu, J., & Ding, Q. (2022). Warming pattern over the Northern Hemisphere midlatitudes in boreal summer 1979–2020. *Journal of Climate*, *35*(11), 3479–3494. https://doi.org/10.1175/jcli-d-21-0437.1

Tian, F., Dong, B., Robson, J., Sutton, R., & Wilcox, L. (2020). Processes shaping the spatial pattern and seasonality of the surface air temperature response to anthropogenic forcing. *Climate Dynamics*, *54*(9–10), 3959–3975. https://doi.org/10.1007/s00382-020-05211-8

Trigo, R. M., García-Herrera, R., Díaz, J., Trigo, I. F., & Valente, M. A. (2005). How exceptional was the early August 2003 heatwave in France? *Geophysical Research Letters*, *32*(10), L10701. https://doi.org/10.1029/2005gl022410

Undorf, S., Bollasina, M. A., & Hegerl, G. C. (2018). Impacts of the 1900-74 increase in anthropogenic aerosol emissions from North America and Europe on Eurasian summer climate. *Journal of Climate*, *31*(20), 8381–8399. https://doi.org/10.1175/jcli-d-17-0850.1

Vautard, R., Cattiaux, J., Happé, T., Singh, J., Bonnet, R., Cassou, C., et al. (2023). Heat extremes in Western Europe increasing faster than simulated due to atmospheric circulation trends. *Nature Communications*, *14*(1), 6803. https://doi.org/10.1038/s41467-023-42143-3

Wang, L., Xu, P., Chen, W., & Liu, Y. (2017). Interdecadal variations of the Silk Road pattern. *Journal of Climate*, *30*(24), 9915–9932. https://doi.org/10.1175/jcli-d-17-0340.1

Wang, Y., Jiang, J. H., & Su, H. (2015). Atmospheric responses to the redistribution of anthropogenic aerosols. *Journal of Geophysical Research: Atmospheres*, *120*(18), 9625–9641. https://doi.org/10.1002/2015JD023665

Watanabe, M., & Tatebe, H. (2019). Reconciling roles of sulphate aerosol forcing and internal variability in Atlantic multidecadal climate changes. *Climate Dynamics*, *53*(7–8), 4651–4665. https://doi.org/10.1007/s00382-019-04811-3

Wu, Z., & Huang, N. E. (2009). Ensemble empirical mode decomposition: A noise-assisted data analysis method. *Advances in Adaptive Data Analysis*, *1*(1), 1–41. https://doi.org/10.1142/s1793536909000047